Front. Struct. Civ. Eng. 2024, 18(7): 1050–1065
https://doi.org/10.1007/s11709-024-1026-x

RESEARCH ARTICLE

Effectiveness of external prestressing in enhancing the non-ductile hanger failure mechanism in reinforced concrete inverted T-beams

Ahmed M. ATTA[a], Reda N. BEHIRY[a*], Mohammed I. HARAZ[b]

[a] *Structural Engineering Department, Faculty of Engineering, Tanta University, Tanta 33511, Egypt*
[b] *Nile Higher Institute for Engineering and Technology, Mansoura 11001, Egypt*
[*] *Corresponding author. E-mail: Redabehiry@f-eng.tanta.edu.eg*

© The Author(s) 2024. This article is published with open access at link.springer.com and journal.hep.com.cn

ABSTRACT Recently, inverted T-beams have been used in reinforced concrete (RC) bridges to support transverse precast stringers. Inverted T-beams, contrary to practice with conventional beams, are loaded on the flanges upper surface. This loading configuration causes hanger failure due to the generation of vertical tensile stresses near the bottom of the web. The key purpose of this study is to investigate the efficiency of vertical external prestressing stainless-steel bars in mitigating non-ductile hanger failure in reinforced concrete inverted T-beams. An experimental study on six inverted-T beams, including two un-strengthened specimens, was carried out. The study showed that the value of the prestressing level had a considerable impact on the performance of hanger mechanism in relation to crack pattern, ultimate loads, cracking behavior, load–deflection, strains, and ductility. The experimental results indicated that the suggested method for strengthening inverted T-beams had efficacy in reducing the seriousness of the non-ductile hanger failure and resulted in a strength increase of up to 53% when compared to that of the un-strengthened specimen. Additionally, two analytical models for estimating the hanger capacity and the average crack width of the strengthened RC inverted T-beams were proposed. The models that were proposed exhibited a high degree of agreement with the experimental results.

KEYWORDS RC bridges, inverted T-beams, strengthening, hanger failure, external prestressing

1 Introduction

Reinforced concrete (RC) inverted T-beams are a common construction solution for many existing RC bridges, as shown in Fig. 1. Clearance restrictions may affect the overall height of the bridge when it is built over a roadway. In conventional rectangular beams, the precast stringer sits on the top of the rectangular section. This method leads to an increase in the overall bridge height, which increases the overall cost. The utilization of RC inverted T-beam involves positioning the precast stringer atop the upper surface of the ledges (bottom flange). This configuration results in a reduction in the overall depth of the bridges and the potential clearance height beneath them.

Precast stringers bearing on the top face of an inverted T-beam's flange create a more complex behavior than that of regular rectangular beams [1–6]. Failures of RC rectangular-section beams may be separated into two distinct types, namely flexural and shear failures. Shear failure can occur even if the beam's flexural capacity is not exceeded, resulting in a non-ductile failure that is marked by its suddenness. This type of failure is considered to be more catastrophic than flexural failure. In contrast, there are six different failure modes that can occur as a result of the position of loads on RC inverted T-beams. These failure modes include flexural failure caused by tension reinforcement yielding, flexural failure caused by top concrete crushing, and overall shear failure in the web near supports. Additionally, there are three other failure modes that may occur, related to the bottom flange: shear friction failure at the interface between the flange and the web, punching shear failure of the flange

Article history: Received Dec 7, 2022; Accepted May 30, 2023

at the point of loading, and failure of the hanger reinforcement responsible for supporting the load up to the compression chord. The six failure modes in RC inverted T-beams are illustrated in schematic form (Fig. 2). When an external load is applied to the bottom flange the most common type of failure that can occur in this setting is known as hanger failure. This particular type of failure is characterized by the development of a vertical breakdown between the web and the flange.

Mirza and Furlong [7] investigated the behavior of one-third scale models of typical inverted T-beams used for bridges in terms of strength and serviceability. The specimens had various reinforcement details and different amounts of hanger reinforcement for the same cross section and approximately the same concrete strength. Of the 27 observed failures, four resulted in pure punching shear failure of the flange, six tests resulted in failures due to pure hanger failure between the web and flange connection, and four tests resulted in failures due to combined hanger failure and punching shear failure. Based on these findings, Raths [8] highlighted some concerns about the safety level provided by the PCI

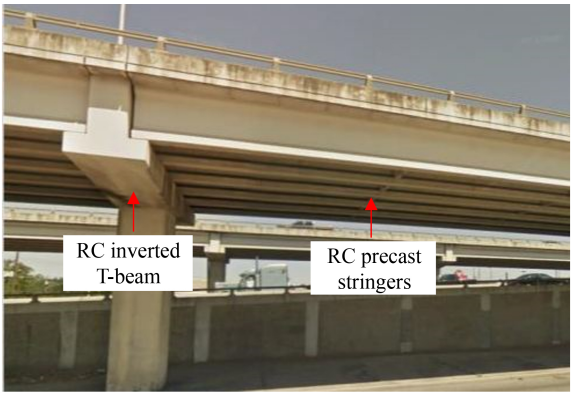

Fig. 1 RC inverted T-beam in bridge.

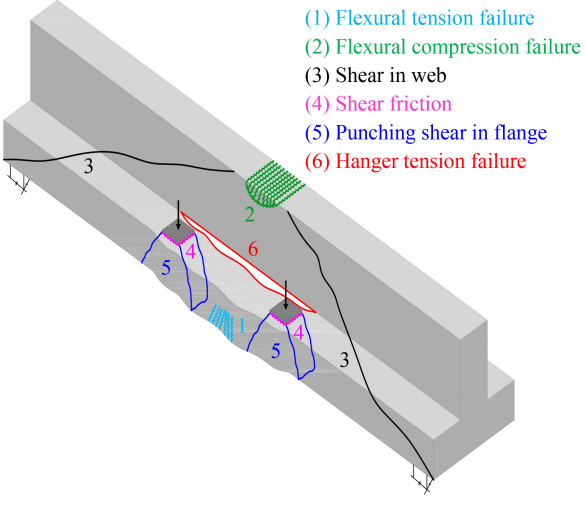

Fig. 2 Possible failure modes of RC inverted T-beam.

equations for the ledge's carrying capacity. The purpose of that research was to review common issues related to inverted L-beams and to develop design recommendations. Raths developed the hanger reinforcement requirement that is addressed in the PCI Handbook [9] and the research recommended using the following equation (Eq. (1)) to calculate the hanger reinforcement (A_{sh}):

$$A_{sh} = \frac{V_u(b_w + e - 0.5)}{\phi f_y(b_w + d'_s - 0.5)}, \quad (1)$$

where V_u is the ultimate applied load, f_y is the reinforcement yield strength, b_w is the width of the web, d'_s is the distance from centroid of hanger reinforcement to the inner web face, e is the distance from the applied load to the inner web face, and ϕ is the strength reduction factor.

Klein [10] conducted an experimental full-scale load test on inverted L-beams. The failure loads were observed to be less than the loads predicted by the current PCI equations. Furthermore, Klein stated that when designing the hanger reinforcement for ledge and web, it is important to consider the eccentricity of the applied load to the centroid of the resisting section of the L-shaped beam. Recently, Garber et al. [11] studied several factors that affect the strength of RC inverted T-beams, including the hanger reinforcement ratio and the thickness of the ledge. That study found that the hanger reinforcement in the web was the key factor for strength. Rizkalla et al. [12] calibrated the specimens tested by Klein [10] using the finite element method (FEM) to confirm its capability relative to the measured behavior. The calibrated models' outputs were in good accordance with the observed behavior. The hanger carrying capacities predicted by the FEM analysis were 90% of the experimental capacities. Also, the calibrated models confirmed that the PCI equations were not conservative in estimating the hanger capacity.

Despite the use of RC inverted T-beams in some existing bridges, which were designed based on older codes [13,14], there has been little study on assessing their strengthening techniques. Externally prestressing techniques were studied in research [15–24] as an alternative to traditional strengthening techniques such as concrete jackets [25–27], steel plates [28–30], or Fiber Reinforced Polymers (FRPs) [31–46]. However, one of the types of failures that may occur when using FRPs in the strengthening is de-bonding, which is an undesirable failure mode. In this case, the FRP materials delaminate from the concrete surface prior to reaching the rupture strain. Therefore, the FRPs are unable to utilize their full tensile capacity. Using a concrete jacket for strengthening the girders in RC bridges leads to an increase in the cross-sectional dimensions, hence an increase in the self-weight. Strengthening using steel plates is widely used for various structural elements. However, steel plates do

not provide a long-term solution due to corrosion issues, especially in applications exposed to severe environmental conditions.

For the purpose of prestressing, a technique known as external post-tensioning involves positioning tendons externally to the concrete element. Because of its many benefits, the use of external prestressing as a technique for strengthening reinforced concrete structures has become more common. The benefits include affordable building practices, uncomplicated monitoring and maintenance, and ease of tendon application. This research presents experimental and analytical studies on the application of external vertical prestressing stainless-steel bars for strengthening RC inverted T-beams to enhance their hanger failure mechanism under symmetric loading.

2 Experimental work

2.1 Test specimens

As presented in Table 1, the experimental work program consists of study of six RC inverted T-beams. There were two reference specimens; B1 without vertical stirrups (hanger reinforcement) at the mid-span; B2 with minimum vertical stirrups at the mid-span acting as hanger reinforcements. There were four strengthened inverted T-beams using external vertical prestressing technique with different levels of prestressing (0%, 30%, 45%, and 60% ε_{py}). The prestressing levels were taken to be similar to earlier studies that involved the strengthening of RC structural elements, which varied from 30% to 60% ε_{py} [47–52].

The specimens were designed based on the formula presented by Mirza and Furlong [7] with the objective of avoiding all types of failure except for hanger failure. The specimens were subjected to simple support with a center-to-center distance of 3000 mm, and had a total length of 3200 mm. It was decided that for all the specimens, the width of the web would be 200 mm, and the total height would be 600 mm. As a preventative step against the possibility of punching shear failure occurring, a flange thickness of 200 mm and a width of 600 mm were decided upon. As can be seen in Fig. 3, both the upper and lower steel reinforcements were the same for all specimens. Fifteen bars with a diameter of 18 mm were used in the T-beam construction process. Nine bars were employed as lower reinforcement, while the remaining six were utilized to fix the stirrups. To prevent shear failure within the web, a series of 10 mm-diameter vertical stirrups were employed, with a spacing of one stirrup per 100 mm and distributed at intervals of 1200 mm from both ends of the specimen. It is noteworthy that specimen B1 was deliberately constructed without the presence of hanger stirrups at the mid-span section. This was done with the aim of investigating the extent to which the existing hanger reinforcement contributes to the load-carrying capacity. Nevertheless, in accordance with ACI 318-19 [53], other specimens were provided with minimal stirrups at the mid-span (8 mm in diameter and placed at 200-mm intervals).

2.2 Material properties

The specimens in the plywood formwork were cast concurrently and subjected to curing with moist burlap. The present study employed ready-mixed concrete comprising 1040 kg/m^3 of coarse aggregate with a maximum size of 20 mm, 760 kg/m^3 of fine aggregate, 400 kg/m^3 of cement, and 160 kg/m^3 of water. Six standard cylinders of concrete, with an average diameter of 150 mm and an average height of 300 mm, were cast and allowed to cure for quality control assessments. The mechanical properties of the concrete, including the compressive strength of the cylinders, modulus of elasticity, and Poisson's ratio, were determined in accordance with ASTM standards [54,55]. In accordance with the previously stated standards, the absolute values for the aforementioned properties were determined to be 29.70 MPa, 26435 MPa, and 0.240, respectively, as presented in Table 2.

The values shown in Table 3 were obtained by tensile testing of the steel bars to estimate the yield strength, ultimate strength, and modulus of elasticity, in accordance with the guidelines prescribed by the ASTM A615/A615M standard [56]. Stainless steel bars with a high strength and a diameter of 12 mm were utilized in order to provide the prestressing force. These stainless-

Table 1 Specimen descriptions

Specimen	Characteristics
B1	RC inverted T-beam without vertical stirrups at the mid-zone
B2	RC inverted T-beam with minimum vertical stirrups at the mid-zone
B3	RC inverted T-beam strengthened with external pre-stressing stainless steel bars at level 0×10^{-6} (0% ε_{py})
B4	RC inverted T-beam strengthened with external pre-stressing stainless steel bars at level 900×10^{-6} (30% ε_{py})
B5	RC inverted T-beam strengthened with external pre-stressing stainless steel bars at level 1350×10^{-6} (45% ε_{py})
B6	RC inverted T-beam strengthened with external pre-stressing stainless steel bars at level 1800×10^{-6} (60% ε_{py})

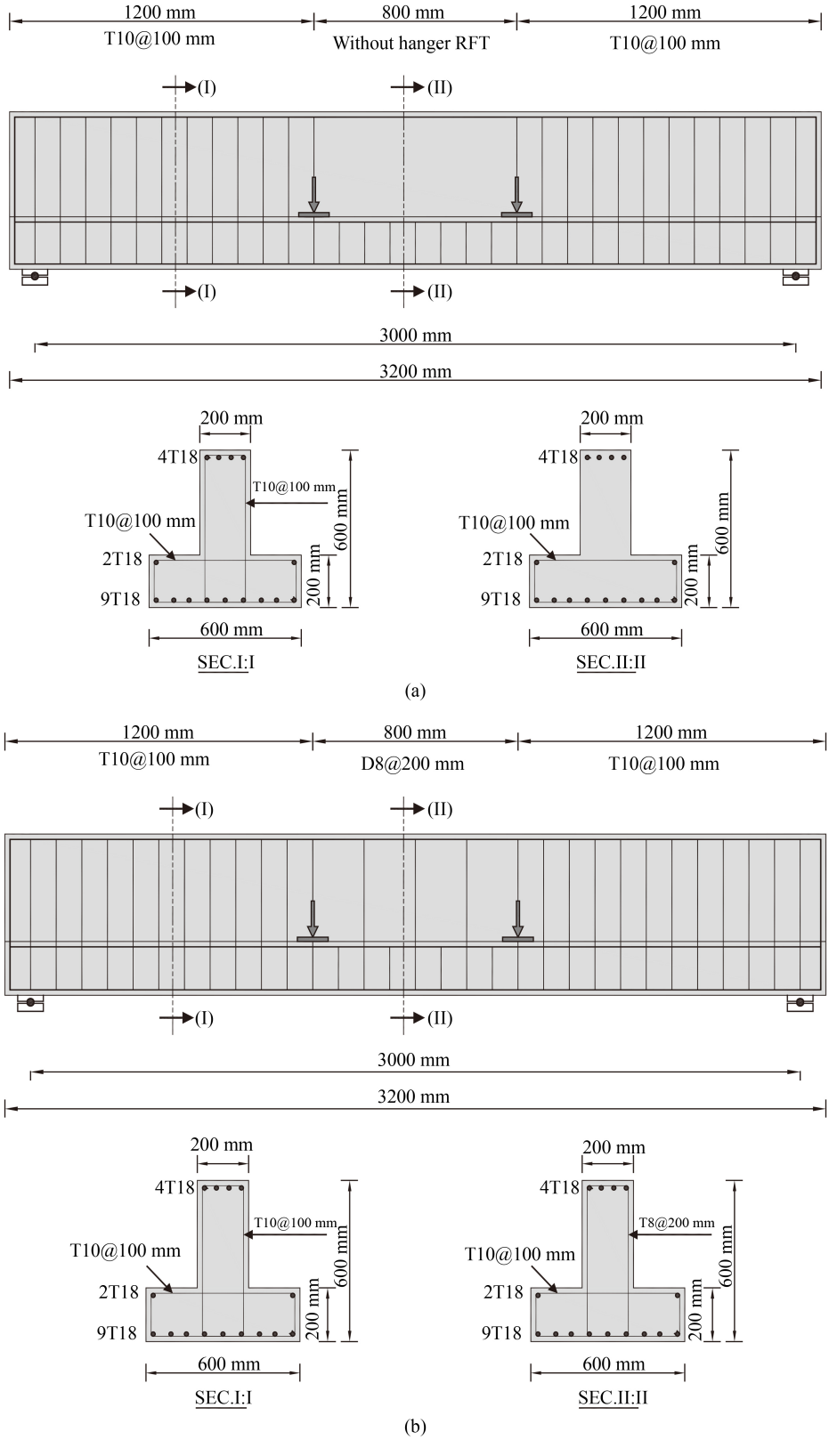

Fig. 3 Dimensions and reinforcement details: (a) specimen B1; (b) other specimens.

steel bars were used in conjunction with mild steel plates that had standard dimensions of 150 mm × 500 mm × 30 mm. To guarantee that the suggested technique of strengthening would be successful, one of the most important steps was to choose steel plates with an appropriate level of flexural stiffness. As a result, the

steel plates were selected with great care to ensure that they had an adequate level of stiffness and to avoid any potential bending deflections. In addition to this, the distance of the clear span between the two stainless-steel bars was deliberately designed to be relatively close to the web formed by the inverted T-beams. The yield strength of the stainless-steel bars was measured at 600 MPa, while their ultimate strength was measured at 740 MPa, and their modulus of elasticity was measured at 200 GPa. The steel plates had a modulus of elasticity of 210 GPa, a yield strength of 255 MPa, and an ultimate strength of 375 MPa.

Table 2 Characteristics of cylindrical concrete samples

Cylinder	Diameter (mm)	Height (mm)	P_{max} (kN)	f'_c (MPa)	E_c (MPa)	υ
Cy. 1	150	300	502	28.40	25098	0.247
Cy. 2	151	300	514	28.70	25608	0.223
Cy. 3	150	300	517	29.26	26234	0.235
Cy. 4	150	300	573	32.40	28863	0.249
Cy. 5	151	301	558	31.15	27753	0.244
Cy. 6	150	300	500	28.30	25052	0.242
Average	–	–	–	29.70	26435	0.240
STDEV	–	–	–	1.69	1553	0.010
Coefficient of variation (COV)	–	–	–	0.057	0.059	0.042

Table 3 Properties of steel material

Diameter, Φ (mm)	Yield strength, f_y (MPa)	Ultimate strength, f_u (MPa)	Yield strain, ε_y ($\times 10^{-6}$)	Young's modulus, E_s (GPa)
8	240	362	1201	200
10	440	623	2178	202
12	600	750	3000	200
18	420	605	2069	203

2.3 Prestressing technique

In this paper, the details of the external prestressing developed by the author are shown in Fig. 4. The external prestressing technique uses six stainless-steel bars, six steel plates, and 12 nuts for each specimen. Two 12 mm diameter stainless steel bars were fastened from the top and bottom of the used steel plates by 14 mm nuts and steel plates with a thickness of 30 mm. The prestressing force was generated using a torque key by tightening the nuts at the bars' ends. A strain gauge was installed on each bar, to control the prestressing level before the test, and to measure the increase in strain during the test. The losses caused by nuts' movements and elastic deformations of steel plates were not considered because the test was performed immediately after the prestressing process.

One of the important aspects that should be considered to simulate the reality of the application of the proposed solution for an existing RC bridge (e.g., the one shown in Fig. 1) is that, before the implementation of the suggested strengthening system, the area of the slab above the strengthened inverted T-beams in-between the two precast stringers should be removed first. After applying the prestressing technique, all removed parts should be cast using a special category of high-performance fiber reinforced cementitious composites (HPFRCC), such as strain-hardening cementitious composites (SHCC), to avoid corrosion attack.

2.4 Test setup and instruments

As shown in Fig. 5, the experimental tests consisted of applying a symmetric four-point loading protocol to all inverted T-beams that only had simple supports. The specimen's tested span was measured to be 3000 mm, while the distance between the loading points was 800

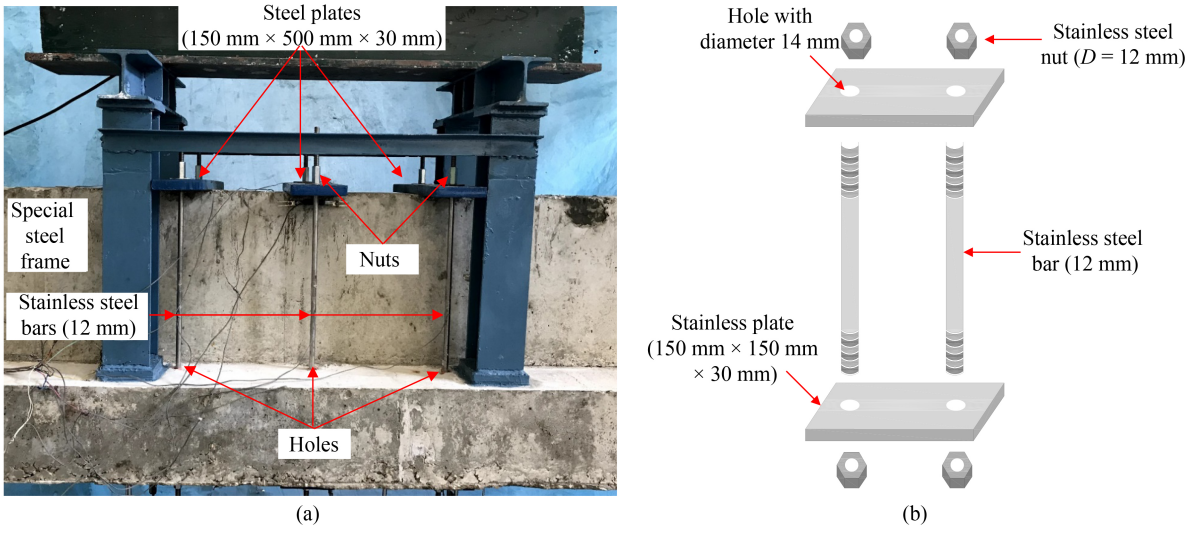

Fig. 4 The external prestressing system: (a) laboratory photo for prestressing technique; (b) schematic for prestressing technique.

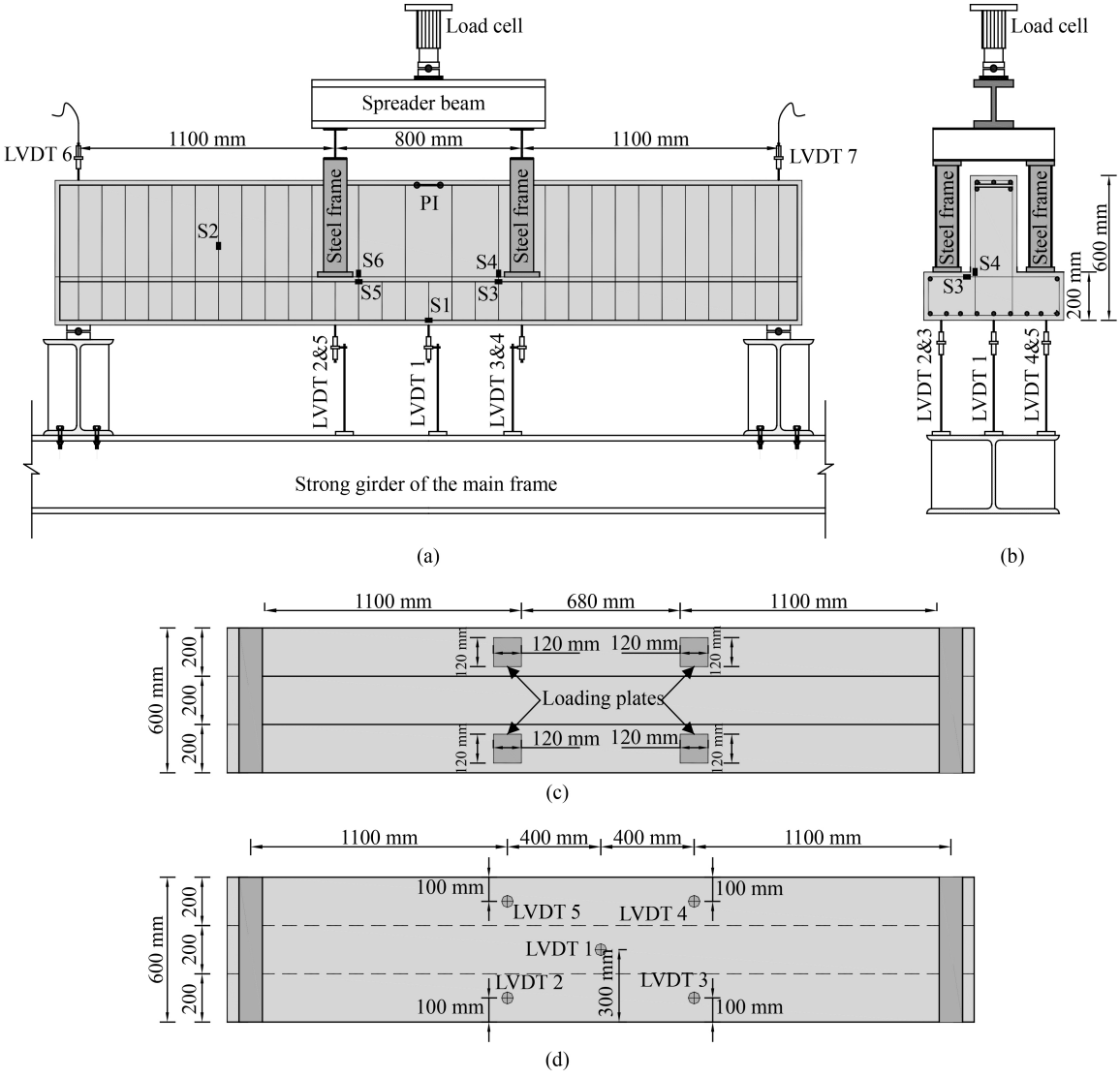

Fig. 5 Test setup and instrumentations: (a) elevation; (b) side view; (c) top view; (d) bottom view.

mm. For all experimental work, a specially manufactured steel frame with high stiffness was designed to uniformly distribute the applied load. The deflection under each loading point was obtained using 100 mm linear variable differential transducers (LVDTs). In addition to this, a pair of LVDTs were fastened atop the supporting points so that they could measure the total net deflection of the specimens that were being evaluated. In order measure the relative displacements between the upper and lower plates, to confirm the stiffness of the steel plates that were used, two LVDTs were mounted beneath them. The results of this measurement were that the relative displacements between the plates were almost negligible. A microscope with a resolution of 0.02 mm was used to measure the width of the cracks at each of the different loading steps. Electrical strain gauges were attached to the stirrup that was placed in the mid-zone, the stirrup that was positioned in the shear span, and the flexural reinforcement that was located in the mid-span. During the period of the test, a π-shaped displacement transducer that was linked to the mid-span concrete surface was responsible for recording the maximum compressive strain that the concrete experienced. During each stage of the test, a data logger device (TDS-150) collected automated recordings of the strains, as well as the loads and vertical displacements.

3 Experiment results

3.1 Crack pattern and ultimate loads

Figure 6 depicts the final crack patterns for all tested specimens. For the control specimen B1, without hanger reinforcement, no cracks were observed in the early stages of loading. At the point that the tensile strain in concrete reached its maximum cracking value, vertical flexural cracks at the tension region appeared. Shortly

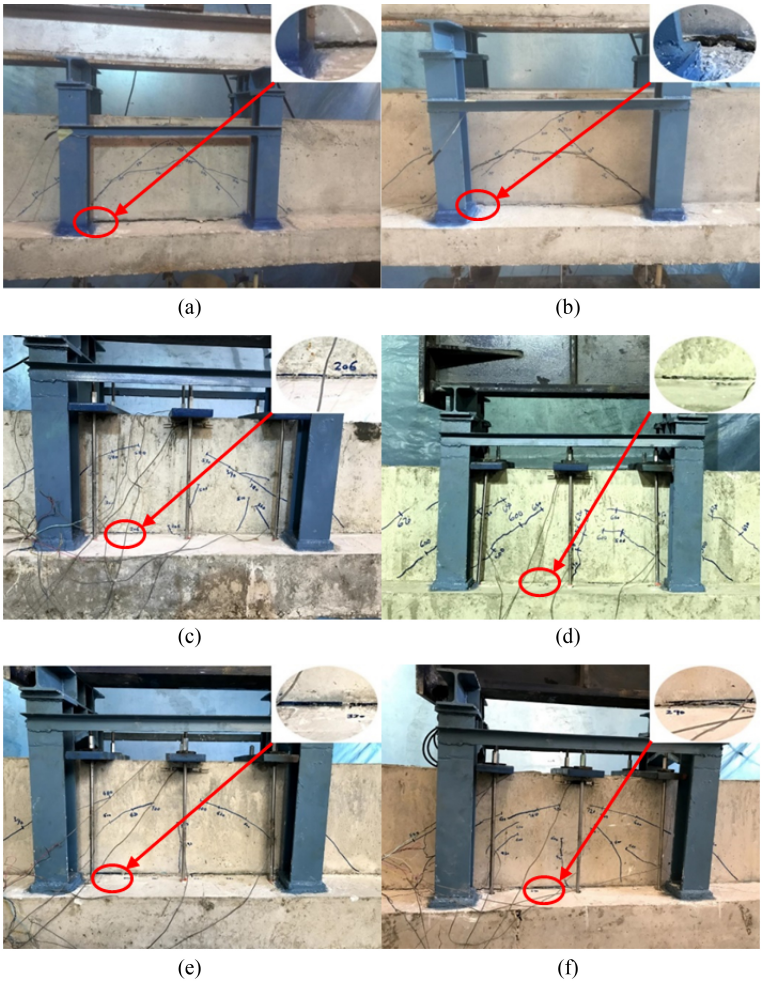

Fig. 6 Final crack pattern for the tested specimens: (a) inverted T-beam B1; (b) inverted T-beam B2; (c) inverted T-beam B3: (d) inverted T-beam B4; (e) inverted T-beam B5; (f) inverted T-beam B6.

after the flexural crack formed, the first crack initiated at the intersection between the web and flange at about 254 kN ($65\%P_u$) and then moved up at an angle of approximately 40° to create arch cracks in the web. As the load increased, the horizontal crack width between the web and the flange increased until the occurrence of non-ductile hanger failure at a load of about 392 kN. The implementation of mid-zone hanger reinforcement, as shown in specimen B2, was able to successfully postpone the appearance of the first hanger cracks (horizontal cracks at the connection between the web and the flange) until a load limit of about 262 kN. In addition to this, the failure mode that was displayed by specimen B2 was somewhat more ductile than that displayed by the control specimen B1. Additionally, when compared to specimen B1, the ultimate load of the tested specimen B2 showed a 23% increase.

Conversely, the prestressing technique had a significant impact on increasing the initial cracking loads and the ultimate loads for all tested specimens, as indicated in Table 4. Furthermore, it was observed that the strengthened specimens exhibited a mode of failure that was predominantly ductile, as opposed to the un-strengthened specimens B1 and B2. The initial cracking loads of the strengthened specimens B3, B4, B5, and B6 exhibited increments of 6%, 23%, 35%, and 48%, respectively, in comparison to B2. The prestressing technique resulted in a rise in the ultimate loads of the strengthened specimens. The specimens B3, B4, B5, and B6 exhibited ultimate loads of 599, 681, 713, and 739 kN, respectively. These values were found to be 24%, 41%, 48%, and 53% higher than the ultimate load of specimen B2.

3.2 Experimental hanger capacity versus analytical estimation

Figure 7 depicts a schematic illustration of the resistance forces that develop throughout the strengthening of inverted T-beams as a result of the prestressing approach. Equation (2) demonstrates that the hanger capacity of RC inverted T-beams that have been strengthened with external prestressing bars is comprised of three distinct contributions. According to Eq. (3) [57], the first contribution (V_c), refers to the resistance that is produced by the

Table 4 Test results

Specimen	Loads				Deflection		Crack width		Initial stiffness (kN/mm)	Strain	
	P_{cr} (kN)	P_u (kN)	Gain in P_u (%) W.R.T B1	Gain in P_u (%) W.R.T B2	Δ_{cr} (mm)	Δ_u (mm)	w_{avg} (mm)	w_u (mm)		In stirrup ($\times 10^{-6}$)	In prestressing bars ($\times 10^{-6}$)
B1	254	392	–	–	2.62	8.01	2.65	7.02	97	–	–
B2	262	482	23%	–	2.30	9.76	1.90	5.31	114	2111	–
B3	279	599	53%	24%	2.20	13.81	1.48	4.89	127	2087	1115
B4	321	681	74%	41%	2.16	8.37	1.03	4.74	149	1695	2641
B5	354	713	82%	48%	2.04	9.55	0.87	3.93	174	1155	3270
B6	389	739	89%	53%	1.74	8.44	0.66	3.54	224	974	4083

Note: W.R.T = with respect to, P_{cr} = the hanger cracking load, P_u = the hanger ultimate load, Δ_{cr} = the mid-span vertical deflection related to P_{cr}, Δ_u = the mid-span vertical deflection related to P_u, w_{avg} = the average crack width related to the service load, and w_u = the crack width related to P_u.

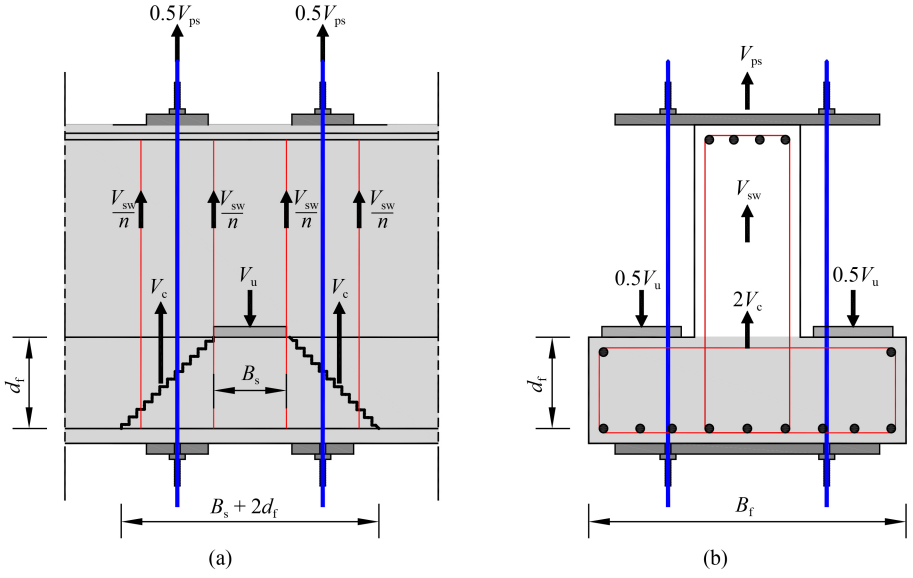

Fig. 7 The generated resistance forces in strengthened RC inverted T-beams: (a) elevation; (b) cross section.

concrete section. The resistance is primarily contingent upon the effective area of the cross section ($B_f \times d_f$) and the average concrete compressive strength (f'_c) of standard cylinders.

$$V_u = 2V_c + V_{sw} + V_{ps}, \tag{2}$$

$$V_c = 0.17\sqrt{f'_c}B_f d_f, \tag{3}$$

where d_f is the flange's effective depth; and B_f is the flange's width. The second contribution of web reinforcement, namely hanger resistance (V_{sw}), is shown in Eq. (4). This contribution is dependent upon the effective depth of the flange (d_f) and the width of the bearing steel plate (B_s). The third term is the contribution of the prestressing strengthening technique (V_{ps}). This contribution depends on the prestressing force in each bar. According to the experimental outcomes, all recorded strain values of the external prestressing bars reached the yield strength and can be calculated by Eq. (5).

$$V_{sw} = \frac{B_s + 2d_f}{S} f_{yw} A_{sw}, \tag{4}$$

$$V_{ps} = f_{ps} A_{ps}, \tag{5}$$

where f_{yw} is the hanger reinforcement yield strength, A_{sw} is the amount of the hanger reinforcement, f_{ps} is the external prestressing bar yield strength, A_{ps} is the amount of the external prestressing bars, and S is the hanger reinforcement's longitudinal spacing. An illustrative representation of the hanger resistance pertaining to the inverted T-beam B6 is provided in Appendix A.

3.3 Load–deflection behavior

Figure 8 illustrates the vertical mid-span deflection and the corresponding applied load for all specimens at each load step. Furthermore, the outcomes of the initial stiffness are presented in Table 4 and were derived from the gradient of the load–deflection graph immediately

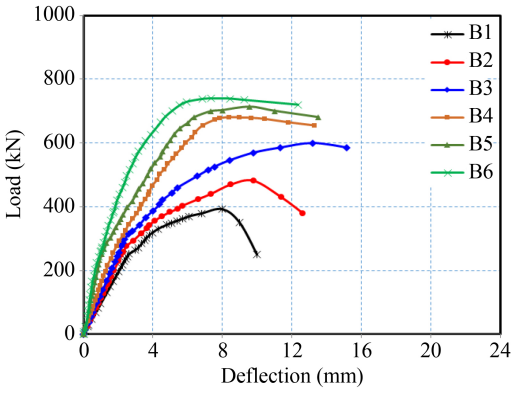

Fig. 8 Load–deflection curves for the tested specimens.

preceding the occurrence of cracking [58]. It is important to keep in mind that, to track post-peak behavior after reaching the ultimate load, the jacking load was gradually released. A bilinear relationship can be used to roughly describe the load–deflection relationship of specimens. The first stage started at the beginning of the test and ended when the initial hanger crack appeared at the connection between the flange and the web. The specimens behaved linearly at this stage, and the initial stiffness depended on the value of prestressing. The second stage began with the when the cracking began and ended with failure. Around this stage, the stiffness began to degrade more quickly, and the load–deflection relationship was affected by the strengthening technique. In particular, at the same load level (480 kN), the implementation of the external prestressing technique resulted in a noteworthy reduction of mid-span deflection, amounting to 75.1% of that for the un-strengthened reference specimen B2. Additionally, as indicated in Table 4, the stiffness of specimens B3, B4, B5, and B6 exhibited a rise of 11.2%, 30.4%, 52.2%, and 96.1%, correspondingly, in comparison to the un-strengthened reference specimen B2.

3.4 Ductility

In comparison to brittle materials, ductile materials possess the ability to undergo inelastic deformation beyond their initial yield points while still preserving their load resistance. This study selectively used two ductility indices, namely displacement-based and energy-based ductility, to assess the ductility effectiveness of the pre-stressing technique. The displacement ductility index (μ_Δ) can be defined as the ratio of the maximum displacement (Δ_{max}) and the yielding displacement (Δ_y), as established by prior research [59]. The energy ductility index (μ_E) is a metric that quantifies the relationship between the energies of a specimen at the point of failure (E_{max}) and yielding (E_y) loads. To obtain additional details, the theoretical computation of the maximum deflection (Δ_{max}) and yielding deflection (Δ_y) was conducted using the methodology recommended by Baraghith et al. [60], as illustrated in Fig. 9. As shown in Table 5, the specimens that were strengthened with external vertical pre-stressed stainless-steel bars showed low ductility. In detail, the strengthened specimens had a loss in ductility of approximately 18% compared to the un-strengthened specimen B2. The main cause of the reduction in ductility was low vertical deflection due to the generated external prestressing force.

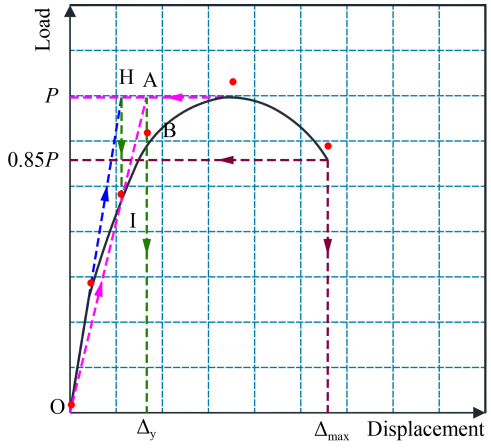

Fig. 9 The yielding load and corresponding deflection [60] (Reprinted from Construction and Building Materials, 327, Baraghith A T, Mansour W, Behiry R N, Fayed S, Effectiveness of SHCC strips reinforced with glass fiber textile mesh layers for shear strengthening of RC beams: Experimental and numerical assessments, 127036, Copyright 2022, with permission from Elsevier.).

The enhancement of load capacity Is a crucial consideration in the strengthening of RC inverted T-beams. The present study involves the computation of the performance factor to ascertain the efficacy of the employed strengthening method. According to Afefy et al. [59], the performance factor (*PF*) can be expressed as the result of multiplying the displacement ductility factor (*DF*) and the strength factor (*SF*). The ductility factor (*DF*) can be defined as the value obtained by dividing the displacement ductility index of a given specimen by the displacement ductility index of the control specimen B1. The strength factor (*SF*) is defined as the ratio of the ultimate load of a given specimen and the ultimate load of the control specimen B1. Specimens that were strengthened with external vertical prestressing stainless-steel bars exhibited greater performance factor when compared to the control specimen B1.

3.5 Strains

The load–strain relationship of the prestressing bars is presented in Fig. 10. The strain values were initially set at levels of 0%, 30%, 45%, and 60% ε_{py}, prior to loading. It is noteworthy that the strain values exhibited a slight

Table 5 Ductility indices

Specimen	Displacement-based ductility					Energy-based ductility					Performance factor		
	Δ_y (mm)	Δ_{max} (mm)	Δ_u	W.R.T B1	W.R.T B2	E_y (kN·mm)	E_{max} (kN·mm)	E_u	W.R.T B1	W.R.T B2	*DF*	*SF*	*PF*
B1	3.39	10.00	2.95	1.00	–	831	2561	3.08	1.00	–	1.00	1.00	1.00
B2	4.62	12.60	2.73	0.93	1.00	1737	5125	2.95	0.96	1.00	0.93	1.23	1.14
B3	5.58	15.12	2.71	0.92	0.99	1904	5260	2.76	0.90	0.94	0.92	1.53	1.41
B4	5.23	13.28	2.54	0.86	0.93	1527	3712	2.43	0.79	0.82	0.86	1.74	1.50
B5	5.39	13.25	2.46	0.83	0.90	2149	4901	2.28	0.74	0.77	0.83	1.82	1.51
B6	5.08	12.35	2.43	0.82	0.89	2602	5698	2.19	0.71	0.74	0.82	1.89	1.55

Note: Δ_y = the mid-span vertical deflection related to the yielding load, Δ_{max} = the maximum mid-span vertical deflection related to the failure load, E_y = energy at the yielding load, E_u = energy at the failure load, *DF* = the displacement ductility factor, *SF* = the strength factor, and *PF* = the performance factor.

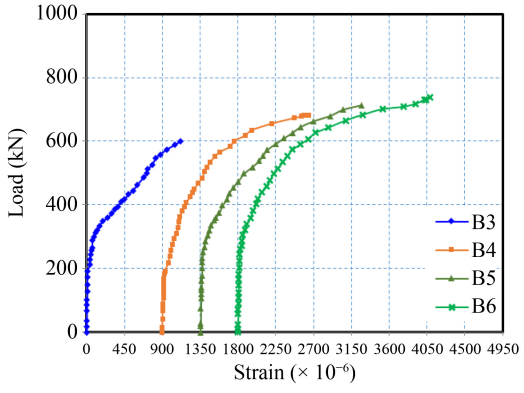

Fig. 10 Load–strain for stainless steel pre-stressing bars.

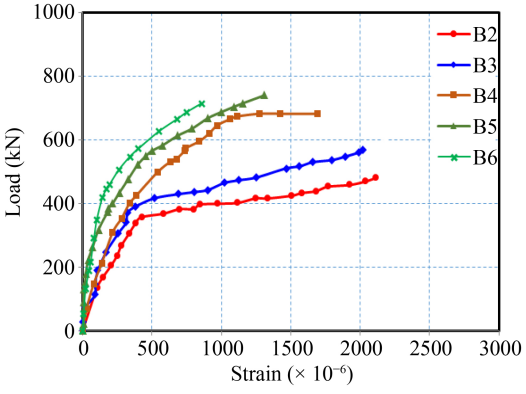

Fig. 11 Load–strain for stirrups in the mid-zone.

alteration prior to the appearance of cracks at the intersection of the web and flange. The minimal strain change in the external prestressing bars can be attributed to the minor deformation assumption, prior to cracking, as predicted by classical elastic mechanics. Following the formation of cracks, the specimen experienced significant vertical deformation and a marked increase in strain due to the tensile stresses. As a result, the hanger resistance is composed of two factors: first, the resistance of concrete is increased by the external vertical compressive stress produced by the prestressing technique, and secondly, the external prestressing bars act as hanger reinforcement to carry the tensile force.

Figure 11 depicts the relationship between the load applied and the associated tensile strain experienced by the hanger stirrups in the studied zone. The load–strain graph for every specimen that was examined demonstrates an initial linear propagation from the origin point down the vertical axis until the occurrence of the first cracking. The behavior that was seen suggests that the employment of stirrups did not improve the ability of the specimen to resist hanger cracking before the initial development of hanger cracks. After the cracking stage, the second part of the relationship between load and strain grew in a way that was't linear up to the stirrup' yielding strain. In other words, a slight plateau was associated with the abrupt opening of cracks. Moreover, the strengthened specimens with externally prestressed stainless-steel bars showed lower tensile strain in the vertical stirrups than in the reference specimen B2 at any load level. In detail, the tensile strain of vertical stirrups at failure for specimen B2 was 2111 × 10^{-6}, while this value for strengthened specimens was in the range of (974−1695) × 10^{-6}.

3.6 Cracking behavior

Different standards set different restriction values for the maximum crack width for aggressive exposure of RC structures because crack width has an effect on the durability of the structure. The maximum crack width is limited to 0.2 mm by CEB-FIP [61] and ECP 203-2020 [62] standards, while 0.30 mm is the limit established by Euro-code [63]. Therefore, it is crucial to investigate the cracking behavior of the suggested strengthening system.

Figure 12 shows the development of the diagonal crack widths of the tested specimens against the applied load. For the specimens strengthened with external vertical pre-stressed bars, only thin visible cracks were observed up to almost 80% of the ultimate loads. In addition, providing external prestressing as a strengthening technique improved the cracking behavior. Thus, at the service stage, strengthened specimens B3, B4, B5, and B6 had smaller crack widths than those of the un-strengthened specimen

B2. The reductions of the average crack widths were 22%, 46%, 54%, and 65% for specimens B3, B4, B5, and B6, respectively, compared to observations for specimen B2. In particular, the extreme crack width for the control specimens at the service load ($67\%P_u$) was found to be 1.90–2.65 mm, but only 0.66–1.48 mm for the strengthened specimens. Finally, it was found that the crack width at the service load was significantly decreased in the strengthened specimens as a result of the compressive force provided by the prestressing technique.

3.7 Analytical evaluation of cracking characteristics for RC inverted T-beams

3.7.1 Hanger cracking capacity (P_{cr})

Herein, a proposed equation is used to estimate the hanger cracking load for the reinforced inverted T-beams (refer to Eq. (6)). A relationship between the normalized hanger cracking capabilities and the prestressing level (μ_{ps}) is established as shown in Fig. 13 to determine the impact of the prestressing level (μ_{ps}) on the hanger cracking load (P_{cr}) of the strengthened RC inverted T-beam. The relationshi's trend line can be utilized to illustrate the impact of the prestressing level ratio via

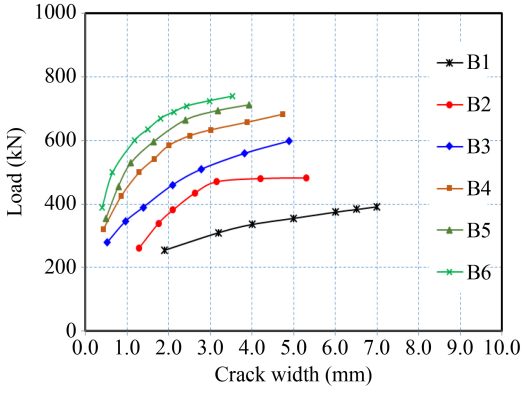

Fig. 12 Crack width against the applied load.

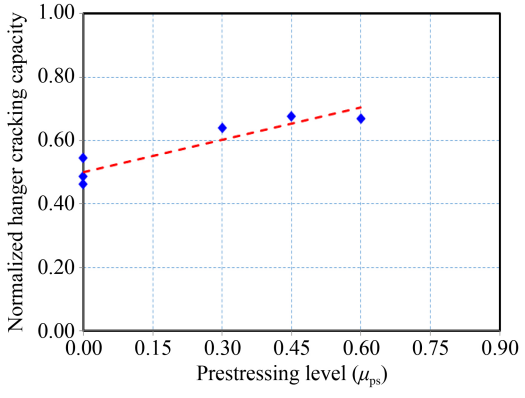

Fig. 13 Normalized hanger cracking capacity versus prestressing level (μ_{ps}).

factor k_{ps}, as presented in Eq. (7). It is noteworthy that the capacities of the experimental hangers were normalized by dividing them by the product of the square root of the compressive strength of concrete ($\sqrt{f_c'}$), the width of the flange (B_f), and the effective depth of the flange (d_f).

$$P_{cr} = k_{ps}\sqrt{f_c'}B_f d_f. \tag{6}$$

$$k_{ps} = 0.50 + \frac{\mu_{ps}}{3}. \tag{7}$$

3.7.2 Average hanger crack width (w_{avg})

Table 6 presents a comprehensive analysis of previous analytical models [64–66] utilized to calculate the average crack width. Table 7 presents the computed average crack width values based on the previously established models, in comparison to the experimental outcomes of the average crack widths for all the tested RC inverted T-beams. It is noteworthy that the experimental outcomes concerning the average crack widths of every specimen were evaluated at the service load level ($0.67P_u$). Evidently, as depicted in Fig. 14, the previously utilized models demonstrate a tendency toward conservative outcomes and have neglected to account for the influence of prestressing levels. Thus, it is imperative to develop a new model that considers such influence. It is important to recognize that the symbols referenced in previous analytical models [64–66] have been clarified in the notation.

(1) Derivation of average hanger crack width formula

The equation proposed for predicting the average hanger crack width of reinforced concrete inverted T-beams was formulated on the basis of strain compatibility and the theory of nearly linear correlations between the mean crack width (w_{avg}), concrete's tensile strain (ε_{ctr}), the hanger reinforcement's tensile strain (ε_{sw}), and the tensile strain of external prestressing bars (ε_{ps}), as presented in Eq. (8). The symbol θ represents the angle of cracking of the crack and can be assumed to be close to zero, as per experimental findings (specifically, the initial crack located between the flange and web, where $\cos\theta = 1.0$). Additionally, the symbol l_w denotes the horizontal projection length of the crack between the flange and web, which is equivalent to the clear distance between the bearing steel plates.

$$w_{avg} = \left[\int_0^{l_w} (\varepsilon_{sw} - \varepsilon_{ps} - \varepsilon_{ctr})\,dx\right]\cos\theta. \tag{8}$$

Equation (9) presents a simplified expression for the average crack width, wherein the influence of tension stiffening is ignored. This is due to the fact that the tensile strain exhibited by the concrete material (ε_{ctr}) is notably lower than that of the hanger reinforcement (ε_{sw}). Thus, it

Table 6 An overview of previous approaches for estimating the average crack width (w_{avg})

Models	Formulas
Witchukreangkrai et al. [64]	$w_{avg} = 0.75 k_w k_p s_{m\theta} \varepsilon_w$ $k_w = \left(\frac{0.004}{\rho_w}\right)^{\frac{2}{3}}$, $k_p = \left(\frac{1}{1+\sigma_{c.ps}/f'_c}\right)$, $s_{m\theta} = \frac{1}{\frac{\sin\theta}{s_{mx}} + \frac{\cos\theta}{s_{my}}}$ $S_{mx} = 2\left(C_x + \frac{S_x}{10}\right) + k_1 k_2 \frac{d_{bx}}{\rho_x}$, $S_{my} = 2\left(C_y + \frac{S_y}{10}\right) + k_1 k_2 \frac{d_{by}}{\rho_y}$
de Silva et al. [65]	$w_{avg} = k_\theta s_{m\theta} \varepsilon_w$
Afefy et al. [66]	$w_{avg} = 0.112 k_s k_t C_s \left(\frac{1}{\rho_w}\right)^{0.207} \left(\frac{1}{\rho_l}\right)^{0.252} (1.25 S_{m\theta}) \varepsilon_w$

Table 7 Experimental average crack widths versus predicted average crack widths

Specimen	w_{exp} (mm)	Witchukreangkrai el al. [64]		de Silva et al. [65]		Afefy et al. [66]		Proposed model	
		w_{avg} (mm)	$\frac{w_{exp}}{w_{avg}}$	w_{avg} (mm)	$\frac{w_{exp}}{w_{avg}}$	w_{avg} (mm)	$\frac{w_{exp}}{w_{avg}}$	w_{avg} (mm)	$\frac{w_{exp}}{w_{avg}}$
B2	1.90	0.48	3.96	0.50	3.79	0.76	2.51	1.86	1.02
B3	1.48	0.48	3.08	0.40	3.70	0.43	3.41	1.32	1.12
B4	1.03	0.48	2.15	0.35	2.96	0.43	2.38	0.98	1.05
B4	0.87	0.45	1.93	0.35	2.50	0.43	2.01	0.81	1.07
B5	0.66	0.45	1.47	0.35	1.90	0.43	1.52	0.63	1.05
Average		–	2.52	–	2.97	–	2.37	–	1.06
STDEV		–	0.997	–	0.801	–	0.700	–	0.036
COV		–	0.396	–	0.270	–	0.296	–	0.034

Note: w_{exp} the experimental average crack width; w_{avg} = the predicted average crack width.

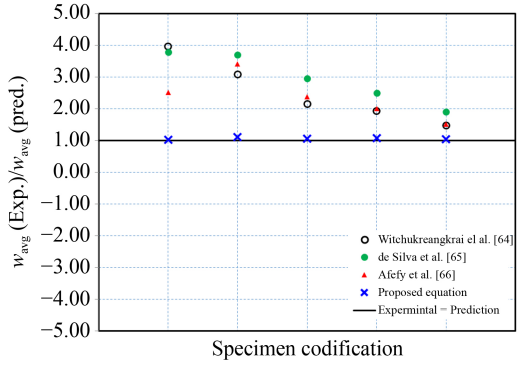

Fig. 14 Estimated average crack width by different models versus experimental data.

is possible to derive the mean crack width by integrating Eq. (9), resulting in the expression shown in Eq. (10).

$$w_{avg} = \left[\int_0^{l_w} (\varepsilon_{sw} - \varepsilon_{ps})\,\mathrm{d}x\right], \tag{9}$$

$$w_{avg} = (\varepsilon_{sw} - \varepsilon_{ps}) l_w. \tag{10}$$

The tensile strain of the internal hanger stirrups (ε_{sw}) is calculated by Eq. (11) where A_{sw} is the total area of internal stirrups, E_{sw} is the internal steel stirrup's modulus of elasticity, and P_{cr} is the hanger cracking capacity load as depicted in Eq. (6).

$$\varepsilon_{sw} = \frac{P_{cr}}{2A_{sw}E_{sw}}. \tag{11}$$

The strain of external prestressing bars (ε_{sp}) is calculated by Eq. (12) where f_{ps} is the yield strength of prestressing bars, E_{ps} is the modulus of elasticity of external prestressing bars and μ_{ps} is the prestressing level.

$$\varepsilon_{ps} = \mu_{ps} \frac{f_{ps}}{E_{ps}}. \tag{12}$$

By substitution into Eq. (10), the calculation of the average width of hanger cracks can be determined using Eq. (13).

$$\begin{aligned} w_{avg} &= (\varepsilon_{sw} - \varepsilon_{ps}) l_w \\ &= \left[\frac{\left(0.50 + \frac{\mu_{ps}}{3}\right)\left(\sqrt{f'_c} B_f d_f\right)}{2A_{sw}E_{Sw}} - \mu_{ps}\frac{f_{ps}}{E_{ps}}\right] l_w. \end{aligned} \tag{13}$$

(2) Experimental crack width versus proposed crack width

Table 7 presents a comparison between the experimental outcomes for the average crack width of RC inverted T-beams and the predicted values derived from the proposed theoretical model. Furthermore, an illustration

of the anticipated average crack width of the strengthened specimen B6 is provided in Appendix B. The mean ratio between the data from experiments and the anticipated results is 1.06, with a corresponding standard deviation of 0.036. Evidently, the aforementioned formula (Eq. (13)) exhibits a high level of precision in estimating the average width of hanger cracks (w_{avg}).

4 Conclusions

The current study investigated the suitability of adopting the vertical prestressing technique in order to improve the hanger failure mechanism for existing RC inverted T-beams under symmetric loading. Six tests were conducted, and the following conclusions were obtained.

1) Strengthening of a RC inverted T-beam that had inadequate hanger reinforcement using external prestressing technique in the hanger zone enhanced resistance to the non-ductile failure mechanism and showed adequate results in terms of both serviceability and ultimate capacity.

2) Using external prestressing technique in strengthening inverted T-beams delayed the appearance of the hanger cracks by about 6% to 48% and reduced the crack width at the service load by about 22% to 65% compared to the values for the same phenomena in the un-strengthened beam B2 based on the value of the prestressing force.

3) The vertical compressive stress generated by external pre-stressed stainless-steel bars can decrease the tensile stress affecting reinforced concrete elements by preventing early-stage cracking. However, they served as a stirrup in the ultimate stage and enhanced the hanger capacity by up to 53% compared to capacity for the un-strengthened beam B2.

4) The proposed strengthening technique showed adequate results from both ultimate capacity and ductility viewpoints; the application of external pre-stressed stainless-steel bars showed an outstanding performance factor that was increased by more than 55% above that for the un-strengthened beam B2.

5) The proposed analytical expressions used to evaluate the capacity of RC inverted T-beams that were strengthened with an external prestressing technique were shown to be satisfactory and conservative; the variation between the experimental capacities and the predicted values calculated from the proposed analytical model was about 1%.

6) The enhanced cracking characteristics of the strengthened RC inverted T-beams (the hanger cracking capacity and the average hanger crack width) were analytically estimated. The proposed models were in good accordance with the experimental results.

It should be clear that, while the results obtained from testing the strengthened RC inverted T-beams are promising, there are a significant number of factors that need to be investigated and confirmed experimentally and analytically to create design guidelines for strengthening the existing RC inverted T-beams by vertical prestressing technique.

Notation

f'_c: the cylinder compressive strength of concrete (MPa)
ε_w: the web reinforcement's tensile strain
k_w: the factor that accounts for the web reinforcement's ratio
k_p: the factor that accounts for the influence of compressive stress ($\sigma_{c.ps}$)
k_1: the bond factor that amounts to 2.4 and 2.0 for smooth and deformed bars, respectively
k_2: the stress distribution's factor that equals 1.2 and 1.0 for vertical and inclined reinforcement, respectively
k_θ: the factor that accounts the angle of inclination of stirrups, 1.2 and 0.80 for vertical and inclined, respectively
k_s: the coefficient considering the web reinforcement hook type
k_t: the coefficient considering the type of web reinforcement
c_s: the thickness of the concrete cover at the side face (mm)
C_x: the longitudinal reinforcement's distance from center line of the cross-section (mm)
C_y: the distance between the cross-sectional central axis and the web reinforcement's interior boundary (mm)
d_{bx}: the longitudinal bar's diameter (mm)
d_{by}: the web reinforcement's diameter (mm)
S_x: the longitudinal bars spacing (mm)
S_y: the web reinforcements spacing (mm)
$S_{m\theta}$: the average spacing between cracks (mm)
S_{mx}: the average horizontal spacing between cracks (mm)
S_{my}: the average vertical spacing between cracks (mm)
ρ_x,ρ_l: the ratio of longitudinal reinforcement (the ratio between the area of the longitudinal reinforcement to the area of the concrete cross-section)
ρ_y,ρ_w: the web reinforcement's ratio (the ratio between the area of the web reinforcement to the area of the concrete cross-section)
θ: the crack's inclination to the horizontal axis

Appendix A

The resistance generated by the concrete section (V_c)

$$V_c = 0.17\sqrt{f'_c}B_f d_f = 0.17\times\sqrt{29.7}\times(600\times156) = 86.7\ \text{kN}$$

The resistance of web hanger reinforcement (V_{sw})

$$V_{sw} = \frac{(B_s + 2d_f)}{s} f_{yw} A_{sw} = \frac{(150+2\times156)}{200}\times(240\times2\times50.3) = 55.7\ \text{kN}$$

The resistance of prestressing bars (V_{ps})

$$V_{ps} = f_{ps}A_{ps} = 600\times(2\times113) = 135.6\ \text{kN}$$

The ultimate hanger capacity (P_u)

$$V_u = 2V_c + V_{sw} + V_{ps} = 2\times 86.7 + 55.7 + 135.6 = 364.7 \text{ kN}$$

$$P_u = 2V_u = 2\times 364.7 = 729.4 \text{ kN}$$

$$P_{exp.} = 739 \text{ kN}$$

$$\frac{P_{u,exp.}}{P_u} = \frac{739}{729.4} = 1.01$$

Appendix B

The hanger cracking load (P_{cr})

$$k_{ps} = 0.50 + \frac{\mu_{ps}}{3} = 0.50 + \frac{0.60}{3} = 0.70$$

$$P_{cr} = k_{ps}\sqrt{f_c'}B_f d_f = 0.70\times\sqrt{29.7}\times 600\times 156 = 357069.0 \text{ N} = 357.07 \text{ kN}$$

$$\frac{P_{cr,exp.}}{P_{cr}} = \frac{389.00}{357.07} = 1.09$$

The tensile strain of the internal hanger stirrups (ε_{sw})

$$\varepsilon_{sw} = \frac{P_{cr}}{2A_{sw}E_{sw}} = \frac{357069}{2\times(2\times 50.3 + 2\times 113)\times 200000} = 0.00273$$

The strain of external prestressing bars (ε_{ps})

$$\varepsilon_{ps} = \mu_{ps}\frac{f_{ps}}{E_{ps}} = 0.60\times\frac{600}{200000} = 0.0018$$

The average hanger crack width (w_{avg})

$$w_{avg} = (\varepsilon_{sw} - \varepsilon_{ps})l_w = (0.00273 - 0.0018)\times 680 = 0.63 \text{ mm}$$

$$\frac{w_{avg,exp.}}{w_{avg}} = \frac{0.66}{0.63} = 1.0$$

Open Access This article is licensed under a Creative Commons Attribution 4.0 International License (https://creativecommons.org/licenses/by/4.0/), which permits use, sharing, adaptation, distribution and reproduction in any medium or format, as long as you give appropriate credit to the original author(s) and the source, provide a link to the Creative Commons licence, and indicate if changes were made. The images or other third party material in this article are included in the article's Creative Commons licence, unless indicated otherwise in a credit line to the material. If material is not included in the article's Creative Commons licence and your intended use is not permitted by statutory regulation or exceeds the permitted use, you will need to obtain permission directly from the copyright holder. To view a copy of this licence, visit http://creativecommons.org/licenses/by/4.0/.

Conflict of Interest The authors declare that they have no conflict of interest.

References

1. Galal K, Sekar M. Rehabilitation of RC inverted-T girders using anchored CFRP sheets. Composites Part B: Engineering, 2008, 39(4): 604–617
2. Cheng H T, Mohammed B S, Mustapha K N. Ultimate load analysis of pretensioned inverted T-beams with circular web openings. Frontiers of Architecture and Civil Engineering in China, 2009, 3(3): 262–271
3. Cheng H T, Mohammed B S, Mustapha K N. Finite element analysis and structural design of pretensioned inverted T-beams with web openings. Frontiers of Architecture and Civil Engineering in China, 2009, 3(2): 148–157
4. Park S H, Cui J, Terzioglu T, Mander J B, Birely A C, Hurlebaus S. Improving existing inverted-T bent caps for serviceability and strength by retrofitting with supplemental steel. Journal of Structural Engineering, 2022, 148(7): 04022084
5. Kim Y J, Alqurashi A. Torsion of carbon fiber-reinforced polymer-strengthened inverted T-beams under combined loading. ACI Structural Journal, 2022, 119(1): 27–40
6. Park S H, Cui J, Mander J B, Terzioglu T, Birely A C, Hurlebaus S. Load balancing external post-tensioning for strengthening existing inverted-T bent caps. Engineering Structures, 2022, 253: 113777
7. Mirza S A, Furlong R W. Strength criteria for concrete inverted T-girders. Journal of Structural Engineering, 1983, 109(8): 1836–1853
8. Raths C H. Spandrel beam behavior and design. PCI Journal, 1984, 29(2): 62–131
9. Prestressed Concrete Institute. PCI Design Handbook: Precast and Prestressed Concrete. 8th Ed. Chicago, 2017
10. Klein G J. Design of spandrel beams. PCI Journal, 1986, 31(5): 76–124
11. Garber D, Varney N L, Gomez E F, Bayrak O. Performance of ledges in inverted-T beams. ACI Structural Journal, 2017, 114(2)
12. Rizkalla S, Nafadi M, Lucier G, Zia P, Klein G. Behavior and Design of Directly Loaded L-shaped Beam Ledges. Technical report RD-16-03. 2016
13. Transportation Officials. Standard Specifications for Highway Bridges. Washington, D.C.: AASHTO, 2002
14. ACI 318-02 & ACI 318R-02. Building code requirements for structural concrete (ACI 318-02) and commentary (ACI 318R-02). Farmington Hills, MI: American Concrete Institute, 2002
15. Ghallab A, Beeby A W. Factors affecting the external prestressing stress in externally strengthened prestressed concrete beams. Cement and Concrete Composites, 2005, 27(9–10): 945–957
16. Shamsai M, Sezen H, Khaloo A. Behavior of reinforced concrete beams post-tensioned in the critical shear region. Engineering Structures, 2007, 29(7): 1465–1474

17. Naser A F, Wang Z. Experimental monitoring of the strengthening construction of a segmental box girder bridge and field testing of external prestressing tendons anchorage. Frontiers of Structural and Civil Engineering, 2012, 6: 308–320
18. El-Shafiey T, Atta A. Retrofitting of reinforced concrete beams in shear using external prestressing technique. Magazine of Concrete Research, 2012, 64(3): 201–211
19. Labib E L, Dhonde H B, Hsu T T, Mo Y L. Shear design of high strength concrete prestressed girders. Frontiers of Structural and Civil Engineering, 2014, 8(4): 373–387
20. Atta A, Khalil A. Strengthening of RC beams with opening in shear zone using external prestressing technique. Magazine of Concrete Research, 2015, 67(3): 133–144
21. Atta A, Taman M. Innovative method for strengthening dapped-end beams using an external prestressing technique. Materials and Structures, 2015, 49(8): 3005–3019
22. Obaydullah M, Jumaat M Z, Alengaram U J, Darain K M, Huda M N, Hosen M A. Prestressing of NSM steel strands to enhance the structural performance of prestressed concrete beams. Construction & Building Materials, 2016, 129: 289–301
23. Xue X, Wang X, Hua X, Wu M, Wu L, Ma Z, Zhou J. Experimental investigation of the shear behavior of a concrete beam without web reinforcements using external vertical prestressing rebars. Advances in Civil Engineering, 2019, 23: 1–13
24. Jia L, Fang Z, Guadagnini M, Pilakoutas K, Huang Z. Shear behavior of ultra-high-performance concrete beams prestressed with external carbon fiber-reinforced polymer tendons. Frontiers of Structural and Civil Engineering, 2021, 15(6): 1426–1440
25. Tena C A, Hernández M O, Archundia A H. Strengthening of reinforced concrete prismatic and haunched beams using light jacketing. Journal of Building Engineering, 2020, 32: 101757
26. Ojaimi M. Experimental study on shear strengthening of reinforced concrete beams using different techniques of concrete jacketing. Basrah Journal of Engineering Science, 2021, 21(2): 53–61
27. Blikharskyy Z. RC beams strengthened by RC jacketing under load. Acta Scientiarum Polonorum Architectura, 2021, 20(1): 25–30
28. Altin S, Anil Ö, Kara M E. Improving shear capacity of existing RC beams using external bonding of steel plates. Engineering Structures, 2005, 27(5): 781–791
29. Mhalhal J, Al-Gasham T, Jabir H. New technique to enhance the shear performance of RC deep beams using mild steel plates. IACSIT International Journal of Engineering and Technology, 2018, 7: 86
30. Suman P, Sarath B, Ramesh K. Strengthening of RC beams with M-sand using external bonding of steel plates. IOP Conference Series. Materials Science and Engineering, 2020, 912(6): 062035
31. Bu L, Shi C, Song L. Consumption of carbon fiber plates in the reinforced concrete beams strengthened with CFPs. Frontiers of Architecture and Civil Engineering in China, 2007, 1(4): 393–398
32. Gand A K, Chan T M, Mottram J T. Civil and structural engineering applications, recent trends, research and developments on pultruded fiber reinforced polymer closed sections: A review. Frontiers of Structural and Civil Engineering, 2013, 7(3): 227–244
33. Hosen M A, Jumaat M Z, Islam A. Inclusion of CFRP-epoxy composite for end anchorage in NSM-epoxy strengthened beams. Advances in Materials Science and Engineering, 2015, 2015: 1–10
34. Hosen M A, Jumaat M Z, Islam A. Side near surface mounted (SNSM) technique for flexural enhancement of RC beams. Materials & Design, 2015, 83: 587–597
35. Darain K M, Jumaat M Z, Shukri A A, Obaydullah M, Huda M N, Hosen M A, Hoque N. Strengthening of RC beams using externally bonded reinforcement combined with near-surface mounted technique. Polymers, 2016, 8(7): 261
36. Shukri A A, Hosen M A, Muhamad R, Jumaat M Z. Behaviour of precracked RC beams strengthened using the side-NSM technique. Construction & Building Materials, 2016, 123: 617–626
37. Hosen M A, Jumaat M Z, Islam A, Salam M A, Mo K H. Side-NSM composite technique for flexural strengthening of RC beams. Computers and Concrete, 2017, 20: 439–448
38. Hosen M A, Alengaram U J, Jumaat M Z, Sulong N R, Darain K M. Glass Fiber Reinforced Polymer (GFRP) bars for enhancing the flexural performance of RC beams using side-NSM technique. Polymers, 2017, 9(5): 180
39. Hosen M A, Jumaat M Z, Alengaram U J, Sulong N R. CFRP strips for enhancing flexural performance of RC beams by SNSM strengthening technique. Construction & Building Materials, 2018, 165: 28–44
40. Hosen M A, Jumaat M Z, Alengaram U J, Sulong N R, Islam A. Structural performance of lightweight concrete beams strengthened with side-externally bonded reinforcement (S-EBR) technique using CFRP fabrics. Composites. Part B, Engineering, 2019, 176: 107323
41. Mhanna H H, Hawileh R A, Abdalla J A. Shear strengthening of reinforced concrete beams using CFRP wraps. Procedia Structural Integrity, 2019, 17: 214–221
42. Shomali A, Mostofinejad D, Esfahani M R. Effective strain of CFRP in RC beams strengthened in shear with NSM reinforcements. Structures, 2020, 23: 635–645
43. Kim Y J, Bumadian I. Strengthening of reinforced concrete beams using embedded carbon fiber-reinforced polymer with polyester-silica. ACI Structural Journal, 2021, 118(4): 31–43
44. Bui L V, Nguyen P T. Shear strength model of the reinforced concrete beams with embedded through-section strengthening bars. Frontiers of Structural and Civil Engineering, 2022, 16(7): 843–857
45. Sengun K, Arslan G. Investigation of the parameters affecting the behavior of RC beams strengthened with FRP. Frontiers of Structural and Civil Engineering, 2022, 16(6): 729–743
46. Hosen M A, Jumaat M Z, Islam A, Al Kaaf K A, Shammas M I, Hakeem I Y, Islam M M. Potential side-NSM strengthening approach to enhance the flexural performance of RC beams: Experimental, numerical and analytical investigations. Structural Engineering and Mechanics, 2023, 85(2): 179
47. Ghallab A H, Khafaga M A, Farouk M F, Essawy A. Shear behavior of concrete beams externally prestressed with parafil ropes. Ain Shams Engineering Journal, 2013, 4(1): 1–16
48. Herbrand M, Classen M. Shear tests on continuous prestressed concrete beams with external prestressing. Structural Concrete, 2015, 16(3): 428–437
49. Qi J N, Wang J Q, Ma Z J, Tong T. Shear behavior of externally prestressed concrete beams with draped tendons. ACI Structural

Journal, 2016, 113(4): 677–688

50. Li Y, Wu M, Wang W, Xue X. Shear behavior of RC beams strengthened by external vertical prestressing rebar. Advances in Civil Engineering, 2021, 2021: 1–12
51. Junlong Z, Dongsheng L. Shear-flexural cracking strength of RC beams with external vertical prestressing rebars: Theoretical investigation and numerical simulation. Advances in Structural Engineering, 2022, 25(3): 593–610
52. Liu Z, Cui Y, Wang W, Cao W, Wang X, Xue X. Strengthening shear resistance of beams without web reinforcements using vertical prestressed steel bars. Advances in Materials Science and Engineering, 2022, 2022: 1–10
53. ACI 318-19 & ACI 318R-19. Building Code Requirements for Structural Concrete (ACI 318-19) and Commentary (ACI 318R-19). Farmington Hills, MI: American Concrete Institute, 2019
54. ASTM C39/C39M-21. Standard test method for Compressive Strength of Cylindrical Concrete Specimens. West Conshohocken, PA: ASTM International, 2021
55. ASTM C469/C469M-14. Standard Test Method for Static Modulus of Elasticity and Poisson's Ratio of Concrete in Compression. West Conshohocken, PA: ASTM International, 2014
56. ASTM A615/A615M-16. Standard Specification for Deformed and Plain Carbon Steel Bars for Concrete Reinforcement. West Conshohocken, PA: ASTM International, 2016
57. Mirza S A, Furlong R W. Design of reinforced and prestressed concrete inverted T beams for bridge structures. PCI Journal, 1985, 30(4): 112–136
58. Khalil A, Etman E, Atta A, Baraghith A, Behiry R N. The effective width in shear design of wide-shallow beams: A comparative study. KSCE Journal of Civil Engineering, 2019, 23(4): 1670–1681
59. Afefy H M, Kassem N M, Mahmoud M H, Taher S F. Efficient strengthening of opened-joint for reinforced concrete broken slabs. Composite Structures, 2016, 136: 602–615
60. Baraghith A, Mansour W, Behiry R N, Fayed S. Effectiveness of SHCC strips reinforced with glass fiber textile mesh layers for shear strengthening of RC beams: Experimental and numerical assessments. Construction & Building Materials, 2022, 327: 127036
61. CEB-FIP. Model Code for Concrete Structures. Paris: European Committee for Concrete, 2010
62. ECP 203-2020. Egyptian Code for Design and Construction of Reinforced Concrete Structures. Cairo: Housing and Building National Research Center, 2020
63. EN-1992. Code for Design of Concrete Structures. Brussels: European Committee for Standardization, 2004
64. Witchukreangkrai E, Meutsuyoshi H, Takagi M, De Silva S. Evaluation of shear crack width in partially prestressed concrete members. Japan Concrete Institute, 2006, 28(2): 823–828
65. de Silva S, Mutsuyoshi H, Witchukreangkrai E. Evaluation of shear crack width in I-shaped prestressed reinforced concrete beams. Journal of Advanced Concrete Technology, 2008, 6(3): 443–458
66. Afefy H M, Baraghith A T, Hassan A, Abuzaid M K. Strengthening of shear-deficient RC beams using near surface embedded precast cement-based composite plates (PCBCPs). Engineering Structures, 2021, 244: 112765